Annals of Biomedical Engineering, Vol. 23, pp. 359–374, 1995
Printed in the USA.

0090-6964/95 $10.50 + .00

An Improved Muscle-Reflex Actuator for Use in Large-Scale Neuromusculoskeletal Models

JACK M. WINTERS

Biomedical Engineering Program, Department of Mechanical Engineering, Catholic University of America, Washington, DC

Abstract—This paper extends the systematic approach described in Winters and Stark (62) for developing muscle models. The underlying motivation is our finding that for larger scale shoulder and head-neck postural systems to be mechanically stable, open-loop muscle properties are often not sufficient. There are three primary contributions. First, the previous muscle mechanical model structure and parameter estimation process of (62) is updated to reflect recent experimental findings. Second, an intrafusal (IF) muscle model is developed that includes a γ_{static} motoneuron (MN) drive, a Hill muscle model, and a muscle spindle sensor across the IF series element; this provides a more appropriate muscle spindle output signal, especially for studies of posture. Third, the conceptual cut between the neurocontrol input and the actuator is raised from just below the MN summing junction to a higher location, allowing a "muscle-reflex actuator" to be defined that satisfies the formal theoretical requirement for possessing passive spring-like behavior when the neurocontrol input is constant. α-γ MN coactivation is assumed, and three types of intrinsic autogenic reflex responses (spindle, Golgi tendon organ, Rhenshaw cell) are developed. Default feedback gains are set based on the criteria that inherent feedback should not sculpt the feedforward excitation drive by more than $\pm 10\%$ of maximum. This new actuator model only mildly affects voluntary goal-directed dynamic performance, but enhances spring-like performance around the postural equilibrium state, in line with available animal and human studies and with several theories on postural regulation.

Keywords—Neuromuscular, Muscle mechanics, Muscle spindle, Posture, Movement, Stability, Biomechanics.

INTRODUCTION

In recent years, three-dimensional (3-D) motion analysis of animal and human movements has become more commonplace. Due to improved computational power, it is also becoming more viable to complement experimental data with simulations that use more realistic, larger scale models, and use numerical optimization to study neurocontrol strategies. This includes natural, goal-directed 3-D movements, such as activities of daily living (ADLs), where the selection from a repertoire of alternative motor strategies is itself an intriguing research question. Equipped with numerical tools such as dynamic optimization complemented by the aggressive use of sensitivity analysis methods (32), it appears that we can now seriously address motor coordination and selection strategies for larger scale systems.

Central to modeling such systems is a model for the system actuator, skeletal muscle (14). Muscle possesses several unique nonlinear properties that allow it to look different under different conditions (63), which may be especially useful for controlling larger scale systems (*e.g.*, creating task-specific virtual subsystems). There is, however, a problem with using conventional muscle models, at least when posture as well as movement is of interest. To simply initiate a simulation run, one must first identify a stable, steady initial posture (29,66). For larger scale systems, this can prove challenging, and theoretically intriguing. We have recently developed a mathematical foundation for postural systems with kinematic and actuator "redundancy" (66) that extends the work of Hogan (22,23). Here we do not assume a preset kinematic configuration, but rather use Forward Static Optimization (FSO) to select between various mathematically viable stable postures that meet certain task requirements (61,66). Central to our approach is that for a postural configuration to be mechanically stable, the total potential energy (E_p) of the system with respect to the n generalized joint coordinates (x_q) must be at a minimum in the n + 1-th order $E_p - x_q$ space. And key to solving this problem is the assumption that muscles possess spring-like properties. This is because a virtual perturbation of x_q causes a change in muscle lengths (mapped via the Jacobian), which, in turn, changes their stored potential energy contribution. We have found that our results are quite sensitive to the assumed quasistatic properties of the muscle actuator. This raises a dilemma. While our muscle model (62) is adequate during voluntary movements, the quasistatic postural behavior of this open-loop model is generally too compliant, especially for inverted pendulum pos-

Acknowledgment—The author gratefully acknowledges the many stimulating discussions with Lawrence Stark (University of California, Berkeley) and Frans C. T. van der Helm (Delft University of Technology), without which this work would not have been possible.

Address correspondence to J. M. Winters, Biomedical Engineering Program, Department of Mechanical Engineering, Catholic University of America, Washington, DC 20064.

(Received 5Aug94, Revised 22Feb95, Revised 3Apr95, Accepted 3Apr95)

tural systems (6,66). There is a need for a reflex-induced contribution to the quasistatic muscle stiffness.

The conventional approach to this need would be to set up a feedback control structure: let the musculoskeletal system be the plant to be controlled, and let the summing junction just before the motoneuronal *final common pathway* level receive converging feedforward and feedback control signals. This provides a convenient and conceptually clean separation of neural and mechanical features; additionally, a measured entity, the electromyogram (EMG), can then be viewed as an indication of the control input signal to muscle (62). Within the engineering modeling community, this approach has been used, with the classic early work being that of Stark (53). It works reasonably well for systems where there are only a few muscles (45,46,53,55,63). The approach of Refs. 59 and 63 is typical. Here, a linear Hill-based model is assumed for muscle, and there is delayed and slightly smoothed feedback of muscle length, velocity, acceleration, length · velocity$^{0.3}$, and force. The length-velocity product relation is based on experimental observations from ramp and hold perturbation studies, describing the region of behavior after the initial transient hypersensitivity to stretch (26). The first four are compared to the kinematic output of a linear unidirectional second order intrafusal (IF) reference model. Feedback gains are estimated on a task-specific basis. However, for larger scale systems such *ad hoc* gain selection becomes conceptually and pragmatically challenging. For example, our current shoulder model includes 95 muscle lines of action (57). If we were to assume a single delayed feedback loop structure with variable (task-specific) gains, we would have to address a 95 by 95 matrix (if assuming all possible connections) or a 95 by 1 vector (if assuming only autogenic connections) of gain parameters. The work of the Loeb-Levine group (18,36) represents one of the few efforts to systematically address feedback gains for complex systems; here optimal regulator theory was used to estimate feedback matrix parameters during tasks such as cat walking. Even this theoretically elegant approach required certain aggressive simplifications, such as the assumption that reflex time delays were insignificant. Consider, however, that experimental estimates of time-delayed reflex gains are usually low (reviewed in Ref. 26). This suggests that for most movement tasks, real-time feedback is used to sculpt mildly a *feedforward* dominated signal (53,61); pathological systems may have inappropriate feedback gains (53). This does not imply that feedback information is not of consequence. Rather, more aggressive responses should be viewed as coordinated multisegmental, task-specific responses that utilize sensory information (43), rather than be forced into the awkward infrastructure of variable reflex gains. Indeed, it might be advantageous to employ a muscle-reflex actuator that includes conservative intrinsic feedback, especially if as a byproduct it could deliver a better estimate of ongoing spindle activity (*e.g.*, for use by subsequent task-specific triggered responses).

These observations have forced us to revisit postural control literature that historically has been separated from movement control approaches that utilize Hill-type muscle models. Classic studies by Liddell and Sherrington (33), and Matthews (38) describe basic muscle-reflex behavior when the autogenic reflex pathways are left intact (called the tonic stretch reflex), and other studies have documented in detail how open loop muscle stiffness differs from the stiffness of a system that includes autogenic reflex activity, especially for lower force levels (21,26). Feldman has long viewed muscle as possessing spring-like properties that help define invariant force-length postural states that are seen experimentally when subjects are given a "do not intervene" command (9,10). He feels strongly that muscle and reflex properties should *not* be considered separately, and views the EMG as an internal byproduct *within* the model rather than as a neurocontrol signal to the model. Houk describes, based mostly on "ramp-and-hold" experimental data involving decerebrate cat preparations, a muscle-reflex "motor servo" that in part serves to regulate stiffness (25,26). Perturbation studies identify quasistatic stiffness fields at the hand (42), and Hogan (22,23) bases much of his theory of impedance control on the assumption that muscles possess spring-like properties. The unifying theme is that, irrespective of possible sources, a muscle with intact reflex activity expresses spring-like behavior that differs from what is seen with an open-loop muscle model, especially for lower force levels. Consequently, in recent simulation studies we have used Hill-type models for movement, and yet felt forced to employ separate heuristic spring-like models to study principles related to posture (66).

Of note is that different experimental protocols may identify fundamentally different types of muscle-reflex "stiffness." Due to intrinsic reflex time delays, the initial "short-range" transient stiffness of a stretched muscle must be a purely open-loop, mechanical response (47). This transient stiffness is dominated by muscle series elasticity, with the contractile machinery serving initially as a "viscous ground" (64,65). It is about an order of magnitude higher than the quasistatic muscle stiffness, and also clearly higher than the steady-state muscle-reflex stiffness (60). There is a need to better characterize the spring-like properties of the muscle-reflex "actuator" with a dependable, synthesized muscle-reflex model that encompasses the various types of stiffness measured experimentally. The purpose of this paper is to address this need.

To synthesize, this concept of a muscle-reflex actuator model represents a significant change in approach and must be pursued carefully. For pragmatic reasons, a new muscle-reflex actuator model should: (i) not dramatically change an existing third order open-loop musculotendon modeling framework that has served us well for a variety

of movement tasks and is currently in common use by several groups; (ii) retain the concept of including only task-independent parameters and a robust model; (iii) include a minimal number of new describing parameters; (iv) retain systematic parameter identification capabilities for all parameters; and (v) include only conservative intrinsic feedback "sculpturing" that could be facilitated by additional task-specific response at the discretion of the user.

METHODS

Overview of Muscle-Reflex Actuator Structure

The modeling structure used here, shown in Figs. 1 and 2, represents a significant extension of the type of approach that we have employed in the past (62). The primary input to the system is still a feedforward neurocontroller signal n_{in}. However, as seen in Figs. 1 and 2, several internal model signals mildly sculpt how neural excitation (n_e) responds to n_{in}, and thus the input n_{in} no longer correlates directly with the EMG or to MN activity. An additional input, n_r, provides a "nominal task reference state" for several of the feedback signals to be defined below. Normally n_r would be shared by a collection of muscles (a "task group," to use the terminology of Loeb [34]), and is based on the common observation that for whatever reasons, motoneuron signals tend to be pulled back toward a nominal reference level (*e.g.*, 10% of maximum) that is related to the postural set (26,61).

A key addition is an embedded intrafusal (IF) muscle spindle model, based on the recommendations found in (59), which, in turn, were an extension of those proposed by Stark (53). The IF is assumed to be skeletal muscle tissue that lies structurally in parallel with the main extrafusal (EF) muscle, in that the relative IF-EF muscle length (strain) changes are directly related. Since it is assumed that the IF system generates insignificant force, there is unidirectional length coupling from the extrafusal (EF) to the IF system (Fig. 1). A classical α-γ (and essentially β) motoneuronal linkage, or α-γ-β coactivation, is assumed. The spindle sensor is assumed to be a transducer that measures strain across the intrafusal series elasticity (SE_{IF}), which is due to SE_{IF} force and thus is not a direct measure of relative EF-IF position error.

The geometric equations relating dimensionless SE extensions and contractile element (CE) lengths are as follows (see also Fig. 2):

$$x_{mt} = \frac{l_{mt}}{l_{m_o}}; \qquad x_{mt\text{-}IF} = \frac{l_{mt\text{-}IF}}{l_{m\text{-}IF_o}}$$

$$x_{ce} = \frac{l_{ce}}{l_{m_o}} = \frac{l_{mt} - l_{t_o} - x_{se} \cdot (l_{m_o} + l_{t_o})}{l_{m_o}};$$

$$x_{ce\text{-}IF} = \frac{l_{mt\text{-}IF} - l_{t\text{-}IF_o} - x_{se\text{-}IF} \cdot (l_{m\text{-}IF_o} + l_{t\text{-}IF_o})}{l_{m\text{-}IF_o}}; \tag{1}$$

$$\text{where} \quad l_{mt\text{-}IF} = l_m = l_{mt} - l_{t_o} - x_{se} \cdot \left(\frac{l_{t_o}}{l_{m_o} + l_{t_o}}\right)$$

where the overall musculotendinous length l_{mt} and SE extensions x_{se} is known, and l_{m_o} and l_{t_o} are the muscle and

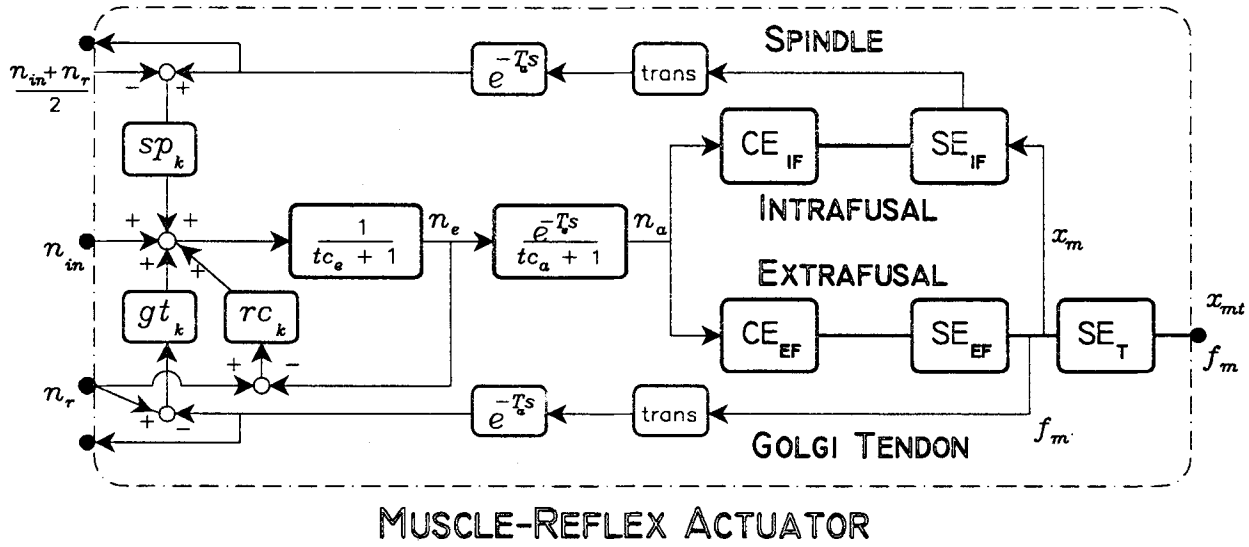

FIGURE 1. Schematic of the overall fourth order, nonlinear muscle-reflex actuator. CNS inputs are n_{in}, the feedforward excitation drive, and n_r, the reference state term related to the general level of coactivation and excitability for a system of muscles. The thicker connection lines represent bicausal mechanical interaction, the thinner lines unicausal information flow. Notice the bicausal coupling between the muscle and its environment, and between the two CE-SE elements. The force generated by the IF system is assumed to be insignificant, thus the unicausal information flow of kinematic information from the EF to IF muscle.

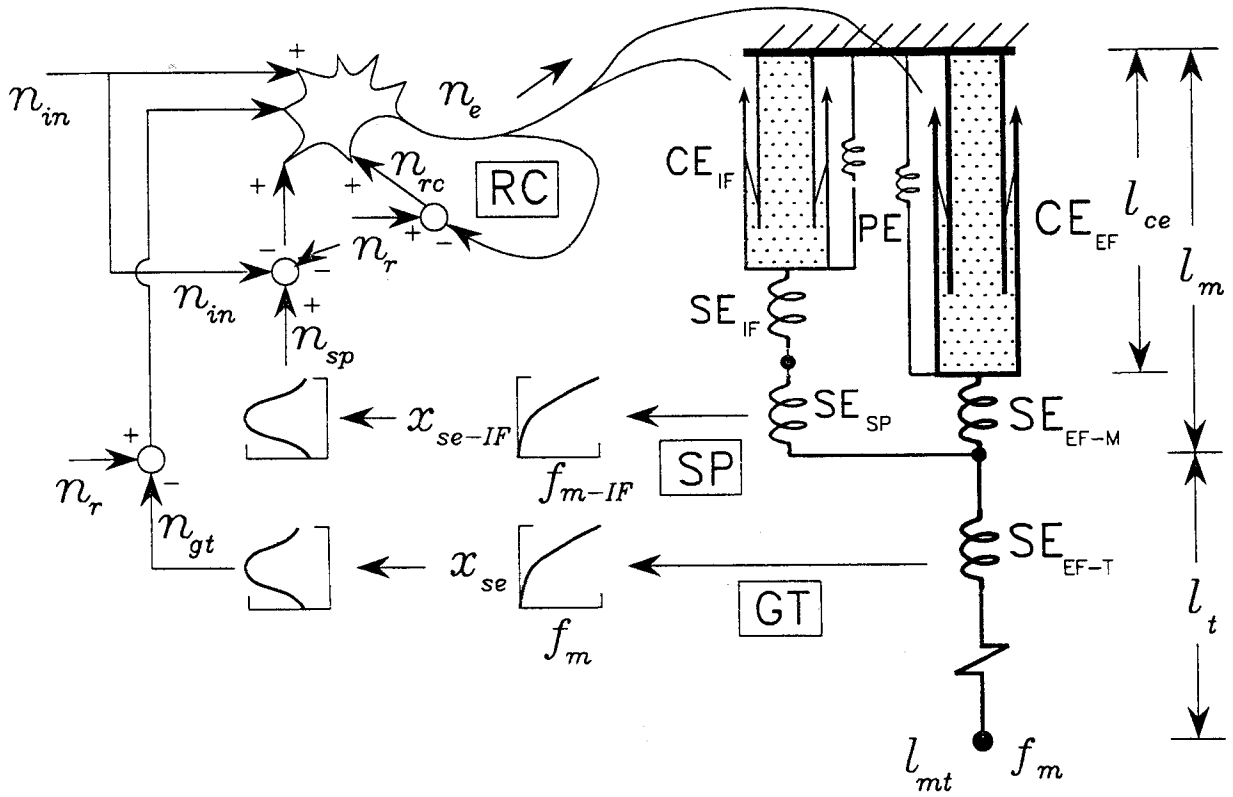

FIGURE 2. Schematic of the structural arrangement of the model, showing EF and IF, and "internal" feedback pathways. The spindle is assumed to be a strain sensor (x_{se-IF}) across part of the SE of the IF system. Static spindle sensitivity is peak in the mid-operating range, dropping off as a normal (Gaussian) distribution to either side, yielding n_{sp}. The spindle "reference value" is a direct function of the feedforward input n_{in} and n_r, rather than any direct measure of length, force, or stiffness (see text). The Golgi tendon organ is also assumed to be a strain sensor (x_{se}), only here for the tendon SE, yielding n_{GT}. The Rhenshaw cell is assumed to provide linear negative feedback to the MN. Both the Golgi and Rhenshaw cell signals are compared to the reference input n_r, thus conservatively pulling n_e back towards n_r from n_{in}. For illustration purposes time delays are not shown.

tendon rest (slack) lengths, respectively. Notice that terms are scaled by l_{m_o} such that as zero force conditions are approached, the two x_{se} terms approach 0.0 and the two x_{ce} terms are 1.0.

The states for the new fourth order muscle-reflex actuator model are: (i) excitation (n_e); (ii) activation/attachment (n_a); (iii) dimensionless extrafusal SE extension (x_{se}); and (iv) dimensionless intrafusal SE extension (x_{si}). When run for forward dynamic simulations (see Ref. 69), the states integrate as follows:

$$\frac{dn_e}{dt} = \{[n_{in} + n_{rf}(n_r, n_{in}, x_{se}, x_{se_{if}})] - n_e\}/tc_e$$

$$\frac{dn_a}{dt} = (n_e - n_a)/tc_a(n_a)$$

$$\frac{dx_{se}}{dt} = [v_{mt} - v_{ce}(n_a, x_{se}, x_{mt})]$$

$$\frac{dx_{se_{if}}}{dt} = [v_{mt_{if}} - v_{ce_{if}}(n_a, x_{se_{if}}, x_{se}, x_{mt})] \quad (2)$$

where n_{in}, n_r, and l_{mt} are inputs (l_{mt} really depends on the system coupled to the muscle), and several ancillary variables that are functions of the four state variables and the inputs are defined: the neural feedback reflex signal $n_{rf}(\ )$ is given by Eq. 11, which in turn requires Eq. 10; the activation time constant $tc_a(\ )$ is defined by Eq. 3; the CE velocity $v_{ce}(\ )$ is given by either Eq. 7 (if shortening) or Eq. 8 (if lengthening), after first satisfying relations defined by Eqs. 5 and 6; $v_{ce\text{-}IF}(\ )$ by a similar set of equations, only for IF muscle; and the IF length $x_{mt\text{-}IF}(\ )$ by Eq. 1. Also, the dimensionless muscle tensile force $f_m(x_{se})$, an output, is given in Eq. 9 (we will postpone multiplication of f_m by the maximum isometric force F_{max} [0.4 MPa · (physiological cross-sectional area)] until the muscle is coupled to an environment). For clarity, the afferent and efferent time delays (see Fig. 1) are not shown explicitly. The last three equations represent muscle dynamics, and can be considered as time shifted from the first equation (for spinal dynamics). Also, n_{rf} in the first equation and n_e in the second equation are from previous times.

When run in inverse dynamic mode, the preferred ap-

proach, uses hybrid optimization (66) and still involves integration of state equations. However, if both f_m and l_{mt} are assumed to be known, it is possible to recursively estimate n_a and n_e. Finding n_a is straightforward: (i) determine x_{se} by inverting Eq. 9; (ii) use Eq. 1 to find x_{ce}; (iii) sequentially use inverse forms of Eqs. 5, 6, 7 or 8, and then Eq. 4 to estimate n_a. To find n_e, numerically differentiate the second equation in Eq. 2.

Several simplifying assumptions were made to keep the model down to fourth order: (i) based on the classic observations of Hill (19,20) and many others, the CE force-length-velocity relation is assumed to be instantaneous, and modulated by the activation level n_a (1,5,20); (ii) there is no node for muscle mass (*i.e.*, as is usual it is lumped into appropriate skeletal linkages [to do otherwise is confounding for large-scale systems where reasonable estimates of linkage mass and inertia are readily available]); (iii) since the IF system generates insignificant force, SE damping is assumed negligible (5), and the strain along the length is assumed uniform, only one state variable (SE extension) is necessary to specify the length of both SE_{EF} and SE_{IF} components; (iv) the passive parallel elements for both EF and IF are assumed to be dynamically-insignificant undamped nonlinear springs which pull (positive force) above rest length and push (negative repulsive force) below it, and attaches as shown in Fig. 2, but generally with insufficient force to warrant separate state variables (in comparison to dynamics between SE and CE); and (v) low-pass dynamics for each of the feedforward and feedback loops are similar and not rate-limiting, and thus a single time constant (tc_e) can be used to characterize neural intrinsic neural dynamics. These assumptions save one, two, one, two, and three possible additional state variables, respectively.

Excitation Dynamics

Excitation dynamics were previously represented by unidirectional first-order dynamics, with a time constant typically on the order of 30 ms (62). This was designed primarily to smooth an idealized neurocontroller input signal n_{in}. In the new model, there are several converging signals to excitation (see Eq. 2): the neurocontroller input drive (n_{in}), and the internal reflex signal that is a function of reference values and delayed sensory feedback signals (n_{rf}), which includes three feedback sources (muscle spindle, Golgi tendon organ, Rhenshaw cell).

The value of the time constant is now reduced to 10 ms, and assumed independent of muscle or motor pool size. This conservative (*i.e.*, low) value is based on the time constant we have previously used for mild smoothing of spindle and Golgi organ feedback dynamics (63) and on reasonable estimates of Rhenshaw cell and spinal neural pool feedforward dynamics (15). Notice that each of these subsystems could have been independently modeled as unidirectional first order processes, but this would unnecessarily add several state variables and parameters of low sensitivity to the model. By assuming the same time constant for each of the dynamic subprocesses and then applying superposition for this linear subsystem, all aspects of simple neural smoothing are encompassed by one time constant.

Activation Dynamics

Activation dynamics (defined as the relative amount of calcium bond to troponin [7,31]) was previously modeled as a unidirectional process with first order dynamics, with n_e as the input and n_a as the output. The rate-limiting step is well known to be related to calcium release, diffusion and uptake (31,67). This had been previously represented by a time constant of about 10 ms during periods of increasing activation and one of about 40 ms for deactivation, with values greater for muscles with primarily slow muscle fibers and larger size (62). This distinction between activation and deactivation dynamics is based on the observation that the underlying dynamic processes differ: activation involves release from the sarcoplasmic reticulum and subsequent diffusion, while deactivation involves an active process of pumping calcium back to the sarcoplasmic reticulum (which requires significant metabolic energy). In reality, both of these processes are occurring simultaneously (67), with dynamics that are a function of the calcium concentration (and thus the activation level n_a).

The following simple model for a variable time constant, based on a simplification of the insights and approach of (37), which has been an available modeling option in the JAMM modeling package of this author since 1989, is suggested:

$$tc_a(n_a) = \begin{cases} tc_{ac} \cdot (tc_{ka} + n_a); & n_e \geq n_a \\ tc_{da}/(tc_{ka} + n_a); & n_e < n_a \end{cases} \quad (3)$$

This relation predicts that as a muscle becomes more activated, the dynamic process slows due to less efficient calcium release and slower diffusion. In contrast, the deactivation rate slows when a muscle is already fairly deactivated (*i.e.*, finding calcium to pump back to the sarcoplasmic reticulum becomes a less effective process [classic Michaelis-Menten chemical kinetics]). Equation 2, with $tc_k = 0.5$, implies that the respective time constants can vary from nominal by a factor of two in either way; reasonable values for time constants are suggested in Table 1. This approach differs fundamentally from that recommended by Zajac (68), in which time constants are assumed to be a function of the excitation drive n_e (or n_{in}) rather than the activation n_a.

It is known that calcium dynamics are also somewhat affected by muscle length; Zahalak refers to this as *tight coupling* (67,37) versus the unidirectional *loose coupling* that was assumed above. The fact that calcium concentration is sensitive to both activation and length appears to

TABLE 1. Default values and definitions for internal parameters within the muscle-reflex model.

Name	Defaults	Comments
tc_e	10 ms	time constant, represents mild smoothing of inputs to n_e
tc_{ac}	15 ms	time constant for activation (mid-n_a range) (range: 10 ms for fast (fc_{sl} = 0) to 20 ms for slow (fc_{sl} = 1) muscle)
tc_{de}	40 ms	time constant for deactivation (mid-n_a range) (range: 30 ms for fast to 50 ms for slow muscle)
tc_{ka}	0.5	dimensionless constant used for activation-dependent scaling of tc_a
fl_{oo}	1.05	dimensionless parameter locating peak of the "Gaussian" relation used for to fit the active component of CE_{fl}, defined for case of peak activation
fl_{sh}	0.4	dimensionless shape parameter for CE_{fl} "normal distribution" curve
fl_{shft}	0.2	dimensionless activation-dependent
$fl_{shft\text{-}if}$	0.3	shift in maximum value on CE_{fl} relation; (0.2 implies that 20% shift to right at zero activation)
$pe_{xm\text{-}l}$	0.6 (len.)	dimensionless parameter (relative to
$pe_{xm\text{-}s}$	0.7 (shr.)	l_{m_o}) that locates point of passive CE_{fl} exponential, where it crosses ±1.0 on dimensionless force axis
$pe_{sh\text{-}l}$	3 (lengt.)	dimensionless shape parameter,
$pe_{sh\text{-}s}$	6 (short.)	passive CE lengthening dimensionless shape parameter, passive CE shortening
fv_{vm}	5.0/sec	maximum unloaded CE velocity (range: 2.5 l_{m_o}/sec for slow (fc_{sl} = 1) to 7.5 l_{m_o}/sec for fast)
fv_{sh}	0.3	dimensionless shape parameter for the Hill equation hyperbola (range [see Fig. 4A]: 0.2 for slow to 0.4 for fast muscle; or constant)
fv_{fml}	0.3	dimensionless max force for lengthening, wrt. isometric
fv_{vml}	0.15	dimensionless lengthening velocity ratio, $*fv_{vm}$, at max eccentric force
fv_{rat}	0.5	ratio of unloaded v_{max} decrement as f_a approaches zero
se_{xm}	0.025	max SE "toe region" strain (see Fig. 6)
se_{fm}	0.4	dimensionless SE force at end of toe region
se_{sh}	3.7	dimensionless shape parameter for toe region
se_{sl}	60	dimensionless slope of SE above toe region (force/strain)
sp_{oo}, gt_{oo}	0.02	maximum transducer sensitivity region on SE strain curves (strain)
sp_{sh}, gt_{sh}	0.02	dimensionless "shape" parameter for SE transducer sensitivity
sp_{kv}	0.1	default rate-sensitivity of spindle transducer
sp_k	0.5	default relative spindle gain (dimensionless)
rc_k	0.1	default Rhenshaw cell feedback gain (dimensionless)
gt_k	0.1	default Golgi tendon feedback gain (dimensionless)
$td_{fd\text{-}a,\text{-}c}$	30, 20 ms	default afferent and efferent feedback loop time delays

Values for IF are the same unless stated otherwise.

help explain the mild (yet important) shifting of the submaximal CE force-length to the right with submaximal activation; this is modeled in the next section.

Attachment Dynamics

This author (60) has distinguished between activation (n_a) and attachment (f_a; the number of attached, mechanically-effective muscle cross-bridge bonds). The original intent of this distinction was to show that the Hill-type muscle model framework can simulate observed phenomena such as the yielding (force drop) seen in some muscles after stretch, presumed to be due to mechanical breakage of cross-bridge bonds (27,41). To do so required an additional first order nonlinear differential equation that determined the attachment f_a as a function of n_a and the CE length l_{ce} (60). The phenomena of yielding, however, appears to be highly variable (3) and less important in a muscle-reflex arrangement (26,60), so at present the added complexity does not appear to be warranted. Yet here we keep the conceptual foundation, and identify f_a with the output of the constitutive (tension-length) relation CE_{fl}, which is well understood at the sarcomere level to be due to actin-myosin fiber overlap (12).

We previously used the sum of a normal (Gaussian, or bell) distribution and a linear slope designed to appropriately skew the normal curve, so that we could fit *measured* force-length, especially for shorter lengths (62). However, Scott and Loeb (49) provide convincing evidence that under 0.7 L_{ceo}, a negative (repulsive pushing) passive force, due to contact between structures at the level of the sarcomere (primarily myosin–z-disc contact), subtracts from the attachment force f_a; this passive repulsive force, modeled in the next section, was previously (accidently) lumped with the active effect. We thus assume that the active CE_{fl} relation can be described by a normal distribution:

$$f_a = CE_{fl}(x_{se},x_{mt},n_a) = CE_{fl}(x_{ce},n_a) = n_a\, e^{-\left[\frac{x_{ce} - fl_{max}}{fl_{sh}}\right]^2} \qquad (4)$$

$$\text{where} \quad fl_{max} = fl_{oo} + fl_{shft}(1 - n_a)$$

where x_{ce} was defined in Eq. 1 and dimensionless parameter values for the optimum length at maximum activation (lt_{oo}) and the spread in the distribution (lt_{sh}) are provided in Table 1 and are used to generate the peak curves in Fig. 3. The assumption of a normal distribution carries theoretical elegance, given the mounting data showing that there is a broad distribution of sarcomere lengths within a muscle, both in series and in parallel (40,58). It is known that as the architectural heterogeneity of sarcomere lengths increases, the length range of effective contraction (represented by lt_{sh}) grows (40,58); the value provided in Table 1 assumes moderate heterogeneity.

Scaling the CE_{fl} Relation. There is an important ongoing

debate regarding how to scale the CE_{fl} curve for submaximal activation (reviewed in Ref. 60). Our past approach, and that of most modeling schemes, assumed multiplicative (vertical) scaling via the activation/attachment input (*i.e.*, that the length at maximum force fl_{max} was independent of the activation n_a [if fl_{shft} in Eq. 5 is zero, then $fl_{max} = fl_{oo}$]). This seems consistent in principle with the cross-bridge model for contraction, yet implies that the unloaded muscle shortens the same amount for any activation, which appears contrary to data which suggests more of a shift in bias (*e.g.*, Ref. 27). Some form of a bias, or "threshold" shift is also suggested by the "postural sate" theories of Feldman (9,10) and Houk (11,25), the foundations of which depend on a γ MN drive and a stretch reflex threshold. Preliminary simulations by this author also strongly imply that the IF system is often not stabilizing if there is no mechanism for bias scaling. Fortunately, there is evidence, on three grounds, that such a mild bias occurs: (i) the firing rate dependent data mentioned earlier (27); (ii) calcium concentrations are both length and activation sensitive, such that at low n_a the CE_{fl} curve shifts to the right (56,58); and (iii) slow muscle fibers are normally the first to be recruited, and the optimum length of slow fibers tends to occur at mildly longer lengths (4,58). The new approach shown in Fig. 3 uses multiplicative scaling and a shift of the length at the maximum active contraction length lt_{max} by up to 20% as the activation decreased toward zero (*i.e.*, $lt_{shft} = 0.2$).

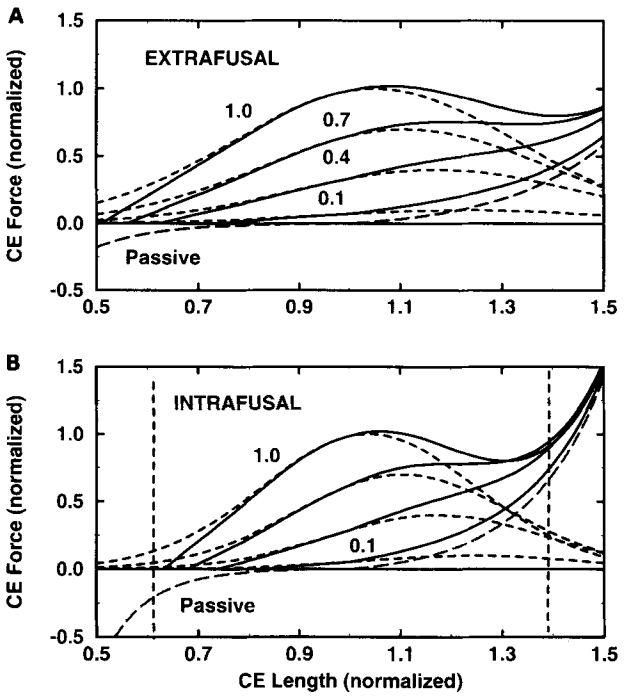

FIGURE 3. Assumed dimensionless CE force-length curves as a function of the activation input n_a. The local passive (activation-independent) contribution is added to the active contribution to determine the net relation. (A) Extrafusal muscle. (B) Intrafusal muscle, where the EF l_{ce} is used for plotting so as the show that the necessary strain in the CE elements for EF and IF will differ. The dashed vertical systems provide the IF strain range that corresponds to the EF range. Here $l_{m_o} = 1.0$, $l_{t_o} = 1.0$, $l_{m\text{-}IF_o} = 0.75$, $l_{t\text{-}IF_o} = 0.25$.

It is suggested that this default CE_{fl} relation be used for all muscles, unless there is experimental evidence that the overlap of the active and passive curves differs from that in Fig. 3 (*e.g.*, more overlap for heart muscle). The key becomes *in situ* estimation of the rest length parameter l_{mo}, which can often prove challenging (*e.g.*, shoulder muscles).

Passive (Parallel) Element

The passive relation for CE lengths above the rest length (*i.e.*, $x_{ce} > 1.0$ by definition) is characterized by the exponential fit that is common for biological tissues under extension (62). For $x_{ce} < 1.0$, we assume that there is a negative (repulsive) force that can subtract from the active force, only with a different dimensional shape parameter $pe_{sh\text{-}s}$ that better fits the data of (49):

$$f_{pe} = PE_{fl}(x_{se}, x_{mt}, n_a) = \begin{cases} \dfrac{1}{(e^{pe_{sh\text{-}1}} - 1)} \left[e^{\frac{pe_{sh\text{-}1}}{pe_{xm\text{-}1}}(x_{ce} - 1)} - 1 \right] & x_{ce} \geq 1.0 \\ \left\langle \left\{ -\dfrac{1}{(e^{pe_{sh\text{-}s}} - 1)} \left[e^{\frac{pe_{sh\text{-}s}}{pe_{xpr\text{-}s}}(1 - x_{ce})} - 1 \right] \right\}, (0.0001 - f_a) \right\rangle & x_{ce} < 1.0 \end{cases} \quad (5)$$

The inequality for shorter muscle lengths is due to the fact that since the overall muscle doesn't push, there is a negative passive repulsive force that is constrained not to be any higher than the current active attachment force f_a (see Fig. 3). Default parameter values, which differ for x_{ce} over 1.0 versus under 1.0 since these are different phenomena, are provided in Table 1. For pragmatic reasons no new state variable is associated with this passive spring, for two reasons: (i) over primary operating ranges PE forces are low, and for most movement tasks is associated with low sensitivity (62); and (ii) due to f_a dependence when shortened, like CE_{fl}, PE is not truly an energy storing spring-like element. This force, f_{pe} enters into the system via its influence on the ongoing applied force that is used below for the CE force-velocity (CE_{fv}) relation. Notice that we assume PE to bridge CE rather than CE-SE; for IF, this is important since otherwise PE is negligible. For most movement tasks, the EF-based f_{pe} can be neglected, or lumped heuristically with joint passive properties (62). However, for our present focus on posture and spring-like properties it is worth modeling, especially for the IF system.

CE Force-Velocity Relation

The form of the CE_{fv} relation is

$$v_{ce} = CE_{fv}^{-1}(f_a, f_{ce}, v_{ce}) = CE_{fv}^{-1}(n_a, x_{se}, x_{mt}) \quad \text{where} \quad f_{ce} = f_m - f_{pe} \tag{6}$$

where the dimensionless muscle force f_m is a function of the state variable x_{se}, and the CE velocity v_{ce} is needed for the formulation of the state equations that is used here (Eq. 2). The equation used for CE_{fv}^{-1} depends on the most recent ongoing v_{ce}, with there being four possible velocity ranges: normal shortening, very high shortening, slow lengthening, moderate and high lengthening. While it is clear that CE_{fv} parameters depend on length (1,5,49) over the primary operating range of most muscles (75–120% of the resting muscle length l_{m_o}) inclusion of such behavior does not appear to be necessary.

CE for Shortening. The CE_{fv}^{-1} relation for *shortening* x_{ce} utilizes the well-known Hill equation (19):

$$v_{ce} = v_{mt}; \quad \text{with } b_m = \frac{0.0001 - f_a}{v_{ce}}; \quad f_{ce} = 0.0001 \qquad v_{ce} < -v_{max}$$

$$\frac{f_{ce} - f_a}{b_m}; \quad \text{with } b_m = \frac{f_a(1 + fv_{sh})}{(v_{max} fv_{sh}) - v_{ce}} \qquad -v_{max} < v_{ce} < 0.0 \tag{7}$$

$$\text{where} \quad v_{max} = fv_{vm}[fv_{rat} + (1 - fv_{rat})f_a]$$

which requires two classic describing parameters: the dimensionless CE force-velocity shape parameter fv_{sh} and the peak unloaded velocity parameter fv_{vm}. The curve is known to depend on the percentage of functionally slow (fc_{sm}) versus "fast" muscle fibers. In Fig. 4A, two strategies are utilized to describe this behavior: a simplification of the approach of (62), where both fv_{sh} and fv_{vm} vary (see Table 1), and an alternative approach in which $fv_{sh} = 0.3$ and the fv_{vm} range is slightly increased; both provide similar behavior over the region of primary physiological interest (*i.e.*, shortening velocities under 0.75 of fv_{vm}). Thus, while most experimental data suggests that the shape parameter is higher in fast muscles, it is also reasonable to assume a set value for fv_{sh} (*e.g.*, 0.25 or 0.3) and mildly increase the range of fv_{vm}, (*e.g.*, from 2 to 8 l_{m_o}/sec). Most muscles have mixed muscle fiber contributions.

CE Force-Velocity for Lengthening. For lengthening muscle, the lower velocity region (by default assumed under 0.15% of v_{max} here [*i.e.*, $v_{max} = 0.15$] is fit by a re-scaled "inverted hyperbolic" relation (62), with higher region by a line with an activation-dependent negative slope (see also Fig. 4):

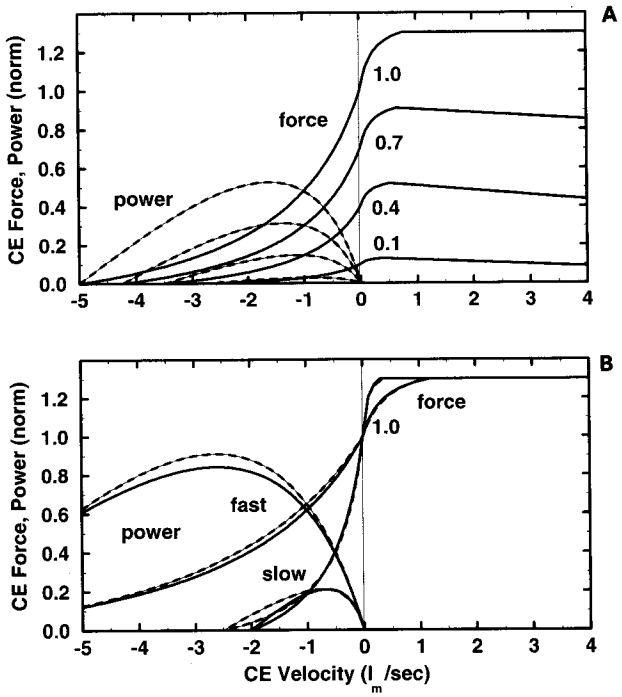

FIGURE 4. (A) Assumed dimensionless CE force-velocity relation, used for the default EF and IF relationships, for several activation levels (solid lines). Muscle power as a function of activation is displayed in dashed lines. (B) Assumed CE force-velocity and power-velocity curves, for "fast" and "slow" extremes in fiber composition: in solid is the case where a constant shape parameter fv_{sh} of 0.3 is assumed and the maximum unloaded velocity fv_{vm} varies from 2 l_{m_o}/sec (slow muscle fibers) to 8 l_{m_o}/sec (fast); in dashed it is assumed that fv_{sh} varies from 0.2 to 0.4, with fv_{vm} equal to 2.5 l_{m_o}/sec (slow) and 7.5 l_{m_o}/sec, respectively. This suggests that it is reasonable to keep fv_{sh} at 0.3 for all fiber compositions, if fv_{vm} is given slightly more variation.

$$v_{ce} = \frac{f_{ce} - f_a}{b_m}; \quad \text{with } b_m = \frac{(fv_{fml} f_a)(1 + fv_{sh})}{(fv_{vml} v_{max})\, fv_{sh} + v_{ce}}; \qquad 0 < v_{ce} < fv_{vml}\, v_{max}$$

$$\frac{f_{ce} - f_a}{b_m}; \quad \text{with } b_m = \frac{fv_{fml} f_a[1 - (1 - f_a)v_{l\text{-}rel}]}{v_{ce}} \qquad v_{ce} \geq fv_{vml}\, v_{max}$$

$$\text{where} \quad v_{l\text{-}rel} = \left(\frac{v_{ce} - fv_{vml}\, v_{max}}{v_{max} - fv_{vml}\, v_{max}}\right) \tag{8}$$

Values for fv_{fml}, the dimensionless upper saturation of force above the isometric value, from 0.1 to 0.8 have been reported in animal studies, although for human studies a tighter range appears to exist of about 0.1–0.4, and from our experience 0.2–0.4. The recent data on cat soleus of (49) provide the best evidence to date that values of 0.3–0.4 are appropriate. With fv_{vml} set to $0.15 \cdot fv_{vm}$, there is a slightly sharper low-velocity transition for lengthening

that for shortening, which is consistent with the common (though still controversial) experimental finding that was first seen by Katz (28) and recently well documented in (49). For velocities above $fv_{vml} \cdot v_{max}$, it is now assumed that instead of remaining saturated at $1.3 \cdot f_a$ for all f_a, the force for submaximal muscle decreases with increasing velocity, but not to a level below the isometric value. This represents a compromise regarding muscle yielding, and is also based in part on this author's observation that predicted behavior for lengthening antagonist muscles using the past model often appeared overly aggressive, with less neural drive necessary to clamp or turn around a system than was indicated by EMGs (13,60). Of note is that there is mounting evidence that there is greater variability in lengthening muscle behavior, both for animal preparations (49) and in human experiments (3). Thus, there is little incentive to refine overly the fit for lengthening muscle.

Unloaded Maximum Velocity (v_{max}) Scaling With Recruitment. As in (62), it is assumed that there is orderly recruitment, with slower muscle fibers (lower v_{max}) recruited first, and thus it is reasonable to scale the peak unloaded velocity (v_{max}) with f_a. Figure 4B, for an EF muscle of mixed fiber composition, shows the approach (see also Eq. 7). This is an important assumption in that it helps justify the assumption of only one input to the motor pool, rather than separate inputs for recruitment and firing rate. For larger-scale systems, this retention of only one dedicated control input signal per muscle becomes an even higher priority.

Series Compliance Element (SE)

As discussed in considerable detail in (60,61), there is series compliance within both muscle tissue and the aponeurosis-tendon complex. The aponeurosis-tendon contribution can be represented by a passive, nonlinear spring. While there has been a concern that aponeurosis and tendon mechanical properties differ significantly (8,34), careful recent evidence suggests that they are indeed quite similar (50). In general, the extension of a tendon during maximal isometric contraction is about 3–5%, with the first 2–3% of extension part of a "toe region" that is well approximated by an exponential function, during which collagen fibers are being "recruited." However, it is now understood (2) that the factor of safety of tendons varies, apparently due to whether the primary function of the musculotendon unit is related to force transmission and impedance modulation (*e.g.*, human wrist muscles, which have less extension and a greater relative toe region) or to strain energy storage and power transmission (*e.g.*, lower limb propulsive muscles).

The peak extension of muscle also appears on the same order, being measured at 2–7%, with a good part of this stiffness dependent on the activation n_a, or more precisely, on the number of attached (recruited) fibers f_a (see reviews in Refs. 20 and 60). The SE force-extension relation is thus not in reality one-to-one (61). Hill (20) also points out that muscle-based stiffness saturates at approximately $0.4 \cdot f_{max}$, which is consistent with the approximate range where all fibers are recruited; such a saturation is also consistent with the "motor servo" data of Houk's group (11,25) and the data of Ref. 21. This reasoning also leads to the concept that the muscle-based series compliance is lower than has generally been utilized in models. Thus, to a reasonable approximation, the muscle-based and tendon-based SE extension contributions are quite similar for all force regions. We thus assume a uniform distribution of SE strain described by the following relation (see also Fig. 5):

$$f_m = \begin{cases} 0.0005; & \text{with } x_{se} = 0.0001; \quad x_{se} < 0.0001 \\ \dfrac{1}{e^{se_{sh}} - 1}\left(e^{\frac{se_{sh}}{se_{xm}} x_{se}} - 1\right); & 0.0001 \le x_{se} < se_{xm} \\ se_{fm} + se_{sl}(x_{se} - se_{xm}); & x_{se} > se_{xm} \end{cases} \quad (9)$$

The shape parameter se_{sh} value of 3.7 (see Table 1) is higher than this author has used previously, but is now

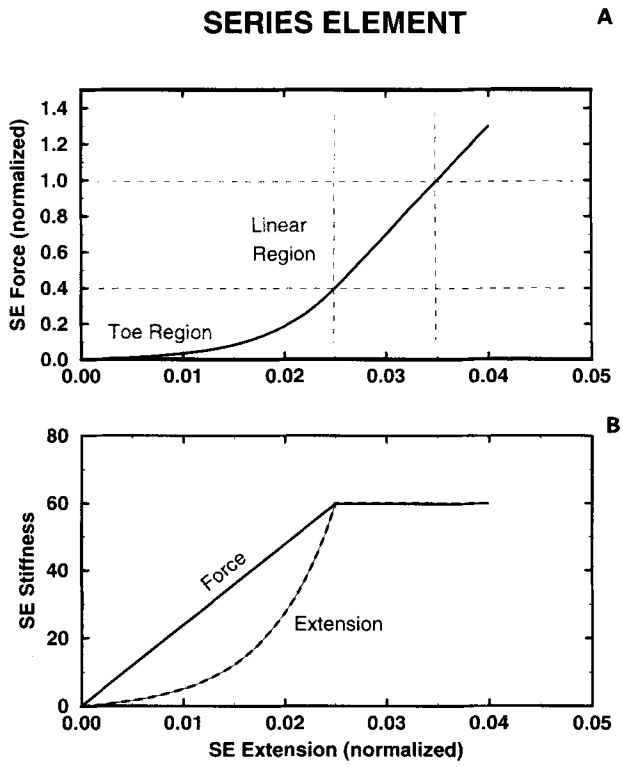

FIGURE 5. (A) Assumed dimensionless SE force-extension curve, with an exponential toe region due to recruitment of collagen fibers in tendon and attached sites in muscle fibrils, followed by a linear region. For a given force, SE extension is assumed uniform along the musculotendinous unit, the same for EF and IF, and independent of the attachment f_a. (B) SE stiffness as a function of SE force and extension.

viewed as more appropriate, and indeed the sharper transition is in retrospect closer to many of the classic muscle studies (*e.g.*, Ref. 20). The IF bridges this relation, but since the IF force is assumed negligible relative to EF forces, the SE relation can be characterized by a single state variable.

In addition to being activation dependent (20), the SE relation is known to be lightly damped (5). In an activating muscle with increasing force ($f_a > f_m$, $df_m/dt > 0$), both of these effects move the force-extension behavior to the left of the nominal curve, although for different reasons (61). Similarly, when both are decreasing, behavior is to the right of the curve. However, changes in f_a and f_m can occasionally be in opposite directions, and thus adding a type of hysteresis doesn't appear warranted.

Model for IF Muscle

Direct data on IF muscle tissue properties is scarce, while indirect evidence based on measurements of spindle afferent firing is voluminous and often in conflict (16,36,38,44). This is in part due to the complexity of the IF infrastructure (both nuclear chain and bag IF fibers, both γ_{static} and $\gamma_{dynamic}$ [and β_{static} and $\beta_{dynamic}$] MNs; both primary [1A] and secondary [II] sensory afferents). The present focus is on posture, and the proposed model is best associated with γ_{static} and β_{static}) MN drive of nuclear chain and bag_2 IF fibers, with secondary (II) afferent transduction. Models for the bag fiber system ($\gamma_{dynamic}$, 1A afferents), under investigation by others (44), would be considered as a complementary system that is also in parallel with EF muscle; it could thus be added separately at a later date.

CE Force-Length-Velocity for IF Muscle. Direct quantitative *in situ* CE force-length and CE force-velocity data for this system is virtually impossible, given how IF tissue is embedded within EF muscle. In principle, the CE_{fl} and CE_{fv} relations for IF could differ from the parent EF muscle. Indeed, γ_{static} MNs tend to have similar functional characteristics to smaller α MNs (*e.g.*, recruited early, often tonically active), and thus could be approximated as similar to a slow EF muscle. An advantage of such a representation is that it justifies a shift of 5–10% in the optimum fiber length (56), which would enhance the region of positive CE_n slope. However, the scant direct data that is available suggests that the muscle tissue innervated by γ_{static} MNs is similar in composition to the parent muscle (reviewed in Ref. 48), both in terms of fiber composition and in terms of sarcomere length and level of heterogeneity. Thus, for CE, we assume as a default that IF muscle behavior is dynamically similar to EF muscle, with one exception: the shift in maximum with submaximal activation is assumed to be slightly higher ($fl_{shft} = 0.3$, versus 0.2 for EF). Notice that since IF fiber bridges only EF muscle and not tendon (Fig. 2), and part of the IF system is passive tissue in series with contractile tissue, the relative percentage excursion range of IF muscle fibers is predicted to be higher than for EF muscle (see Fig. 3).

PE for IF Muscle. To satisfy our objectives for postural regulation, it appears to be of fundamental importance that the IF force-length slope, as felt by the spindle sensor, be positive (9,22,25,66). The data on spindle firing (21,35,39,48) and "do not intervene" experiments (9,10,26) provide indirect evidence that it is. This leads to the conclusion that the PE is of importance for IF muscle, and to the assumption that PE bridges CE rather than CE-SE, since its force contribution is then felt by the spindle sensor. We have little knowledge about PE for IF muscle, and thus it is assumed here to be similar to that for the parent EF. However, it is surmised that it might be stiffer (with respect to IF force generation).

SE_{IF} and Spindle Measurement. As with SE_{EF}, SE_{IF} is also assumed to be divided into two components, with length measurement taken from a part of the functional IF "tendon" at the nuclear chain (Fig. 2). The scant data that is available suggests that the SE_{IF} strain in the region of the sensor is similar or perhaps more compliant than the parent EF. The stiffness of the sensing area is assumed the same as for the rest of the system, with uniform SE strains along the IF length that are assumed to be the same as for EF. Since the spindle sensor is assumed to measure strain, which is assumed to be uniform along the fiber, distributing the SE extension between muscle and the spindle sensing region becomes irrelevant. Notice in Fig. 6B that there is an inherent nonlinear sensitivity toward relative SE forces below about 0.2 (see also Fig. 2). At present, the viscous nature of the nuclear chain (and bag_2) is assumed negligible.

Sensory Strain Gages: Spindle and Golgi Tendon

Both the muscle spindle and Golgi tendon organ are viewed as strain gauges measuring across part of a SE element (see Fig. 2). Because of the higher relative extension change for lower forces (see Fig. 5), the force sensitivity is higher for lower forces even though the transducer is assumed to measure length linearly. Based on the review by Loeb (35), it is assumed that the sensitivity is highest in the mid-strain range (0.02), and can be fit by a standard bell-shaped normal (Gaussian) tuning curve. Thus, the sensor outputs are given by:

$$n_{sp} = \frac{1}{sp_{rng}}\left[n_{sp_0} + sp_{kv}\frac{dn_{sp_0}}{dt}\right]$$

$$\text{where} \quad n_{sp_0} = e^{-\left[\frac{(x_{se\text{-}IF} - sp_{oo})}{sp_{sh}}\right]^2} \tag{10}$$

$$n_{gt} = \frac{1}{gt_{rng}}\, e^{-\left[\frac{(x_{se} - gt_{oo})}{gt_{sh}}\right]^2}$$

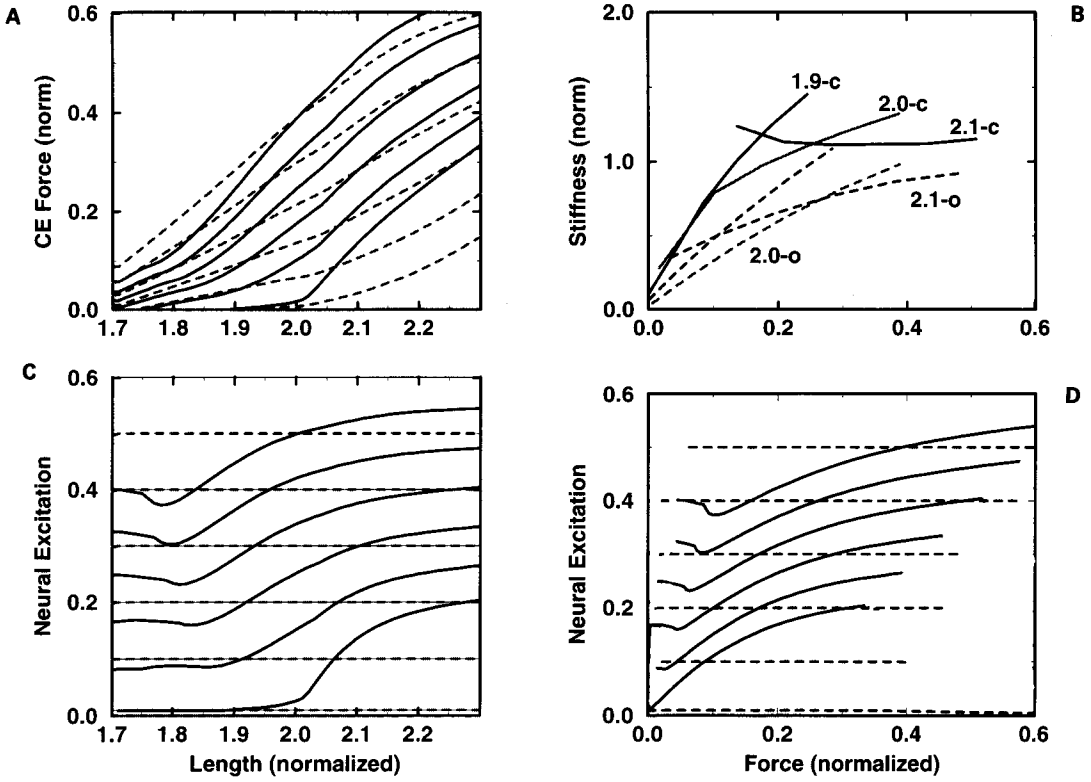

FIGURE 6. Dimensionless quasi-static behavior of both the open-loop muscle model and the new muscle-reflex actuator for constant postural state excitation inputs n_{in} of 0.01, 0.1, 0.2, 0.3, 0.4, and 0.5, and for a musculotendinous actuator with $l_{t_o} = l_{m_o} = 1.0$, and thus a total musculotendinous slack length of 2.0 units, and $l_{m\text{-}lF_o} = 0.75$, $l_{t\text{-}lF_o} = 0.25$. The emphasis on the lower region of n_{in} is because this is the region that is by far the most common in everyday life. (A) Force-length postural curves (dashed: open-loop extrafusal muscle model, solid: muscle-reflex actuator). (B) Neural excitation n_e versus musculotendinous length l_{mt} for both open-loop (dashed) and muscle-reflex (solid) actuators. (C) Overall static stiffness versus muscle force for three l_{mt} crossings (1.9,2.0,2.1); the three curves that are nearer the origin are the open-loop cases (−o), the highest three muscle-reflex cases (−c). (D) Neural excitation n_e versus muscle force for both types of actuators (muscle-reflex in solid, open-loop in dashed).

where typical parameter values are provided in Table 1, and the division by the physiological range (sp_{rng}, gt_{rng}) represents a simple mapping, with a 0.0 strain representing zero firing, 0.04 peak sensor firing. The spread for the tuning curve, sp_{sh} and gt_{sh}, was defined such that the SE strain extremes (0.0, 0.4) are about 37% as sensitive as the sensor mid-region (sp_{oo},gt_{oo}). These signals are available both for use by reflexes and for other purposes (*e.g.*, triggered responses, off-line learning).

Notice that for the spindle, a rate sensitive transducer term is also included, though as a separate channel with a very low gain (see Table 1). For practical purposes, most of the observed rate sensitivity is really a mechanical effect related to CE nonlinearity and CE-SE bicausal interaction, and not strain transducer characteristics. Simulations back up this assumption. Note that the proposed spindle model is not intended to capture the effects of a $\gamma_{dynamic}$ MN drive.

Reference Values and Feedback Gains

Unlike for mechanical properties, systematic parameter identification is in principle not possible for neural structures. There are two types of parameters. First, to be useful, each signal should also be compared with some reference state level; this bias drive sets the stage for both positive and negative influence of sensory information (35). Second, there must then be a feedback gain that works on these error signals. The following simple form is assumed here:

$$n_{rf} = sp_k\left[n_{sp} - \frac{(n_{in} + n_r^*)}{2}\right] + gt_k(n_r^* - n_{gt}) + rc_k(n_r - n_e) \tag{11}$$

Notice that the reference values are hypothesized to be simple functions of neural inputs as opposed to the output of a dynamic reference model. The system-wide *task reference state input bias*, n_r, represents the current default MN drive for a task group of muscles. It can be thought of as a compromise between three factors: (i) the desire for a centrally biased activity level so that inhibition as well as excitation is possible (35); (ii) the desire to minimize metabolic energy consumption; and (iii) functional performance needs such as impedance modula-

tion (22,23,65). Values of 0.05–0.3 are suggested. The value for n_r^* represents inverse SE mapping, as if n_r represented f_m: with $n_r = 0.2$, from Fig. 5 we see that $n_r^* = x_{se}/xx_{se\text{-}mg} \simeq (0.02/0.04) = 0.5$, which is a perfectly centered signal on the interval ⟨0,1⟩. In each case n_e is pulled mildly toward n_r from n_{in}, the amount of which depends on the feedback gains.

The default gains rc_k and gt_k are both 0.1 (table 1) (*i.e.*, the maximum of pull on n_e is 10%); in practice, n_e is rarely sculpted downward by more than 0.06 or upward by more than 0.02 by each. Usually Rhenshaw and Golgi effects are complementary. However, for voluntary initiated movements, Rhenshaw feedback tends to be faster to develop, while for external perturbations, Golgi feedback develops first.

For the spindle, a reasonable approach is to bias the desired reference toward n_{in}; Eq. 11 provides a simple form that turns out to be conservative and yet effective, and adds no new neural parameters. The default reflex gain sp_k was set through simulations, based on the design criteria of ±10% effect over a reasonable local position operating range (*e.g.*, ±10% length change). Of note is that there appears to be evidence for mild multiplicative gain modulation with postural "set" (26), and as well as control theoretic reasons (61); however, we will see that even the simpler form used here is quite effective.

RESULTS

The primary motivation behind this project was the need to enhance postural stiffness within large-scale musculoskeletal models. Figure 6 documents the steady-state stiffness of the new muscle-reflex model versus the open-loop muscle model. From Figure 6A and B we see that a series of "invariant" lines emerge that do not cross. It is important to recognize that the stiffness is especially enhanced for lower levels of n_{in} drive, and especially below 0.2. This is in fact the operating region for the classic "do not intervene" studies of Feldman and colleagues (9,10) and related studies by Houk and colleagues (reviewed in Ref. 26). Notice especially the curves for $n_{in} = 0.01$ and 0.1—due to the SE relation being nonlinear and the spindle being assumed to function as a strain transducer, this is a sensitive region where n_e can rise dramatically. It is in these lower regions that we needed increased static stiffness for our studies of large-scale postural stability, and as seen in Fig. 6C, we have it. Since n_{in} is constant, the solid lines in Fig. 6A represent true static spring-like behavior (*i.e.*, the input, n_{in}, is not changed by an external perturbation or by reasonable internal model assumptions such as an attachment-dependent SE). The user is thus relieved of the burden of producing *ad hoc* feedback to achieve meaningful postural behavior. The role of Rhenshaw and Golgi feedback is predictable: mild biasing of the n_e signal from n_{in} towards the reference level n_r. In fact, sustained n_e levels above 0.5 are rare, except perhaps for certain athletic events; these channels can be viewed as a mechanism gently pulling n_e away from extremes. The effect on dynamic performance is very minor; it is the spindle-based reflex that is critical for postural stiffness. For some applications, these loops may not be of interest and can be turned off by setting rc_k and gt_k to zero.

For the typical isolated muscle "ramp and hold" perturbation experiments, we see that feedback does in fact moderately influence behavior, in a predictable manner, by mildly enhancing the stiffness once the 50 ms time delay is past (Fig. 7). The sudden jump in the feedback signal after the time delay reflects the intrinsic "short range stiffness' of the CE-SE IF system, rather than sensor sensitivity to velocity or acceleration. Simulations involving stretches at other velocities, not provided here, and sensitivity analysis studies, make this clear. Notice that the general effect exists for different lengths, different input levels n_{in}, and both shortening and lengthening

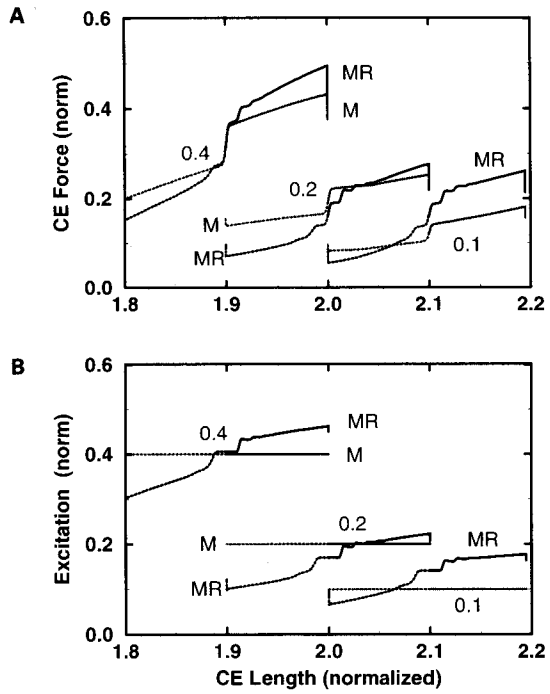

FIGURE 7. Transient behavior of the open-loop extrafusal muscle and of the muscle-reflex actuator during "ramp and hold" length inputs, for several different initial musculotendon dimensionless lengths (l_{mt_o} = 1.9, 2.0, 2.1, where $l_{m_o} = l_{t_o} = 1$) and feedforward inputs ("postural states") n_{in} (0.1, 0.2, 0.4). In each case, the lengthening or shortening velocity ramp of ±0.2 l_{mt_o}/sec (±0.4 l_{m_o} sec) is applied, which is stopped after a displacement of 0.1, and held at this new position. There are 12 runs in all, 6 shortening and 6 lengthening, at each initial position both for muscle alone (M) and for the muscle-reflex (MR) actuator. For simplicity in seeing distinctions in slope, for these runs fl_{shft} is set to 0.1. (A) Dimensionless force f_m versus length. (B) Neural excitation n_e versus length.

ramps. In general, the order of the effect on n_e is about 5–10%, with more relative sensitivity at lower levels of n_{in}. As expected, due to the enhanced reflex stiffness, the model has less of a tendency to drift. The vertical line at the end of each trace in Fig. 7B is a measure of the change in n_e once the ramp ends and the new position is held. Lower velocity "ramp and hold" show similar trends in Fig. 7. Higher velocities also provide behavior that was as expected, with one exception: somewhat unstable behavior for the special case of very high lengthening velocities when n_{in} is low. This is due to the drop in force at high velocities (see Fig. 4B).

A key objective of the modified model was to retain "open-loop" performance during voluntary movements, while enhancing model behavior during external loading, and for steady-state postural regulation. As expected, and indeed virtually guaranteed through the modeling infrastructure and the use of conservative feedback gains, the autonomic reflex activity provides only mild sculpturing of the n_e signal during voluntary movement, with n_e closely resembling the feedforward n_{in} signal. This was a general finding. As is often seen experimentally, the sensitivity to external perturbation during a movement is sometimes enhanced. Thus, the integrity of the previous model, for voluntary goal-directed, predictable movements, is retained. However, it is worth noting that n_{in} is no longer as easily interpreted as a force-type input to a muscle filter; it represents an excitation drive state that is not easily reduced to force, position, or stiffness.

DISCUSSION

A newly defined muscle-reflex actuator is proposed that encompasses behavioral traits of both the open-loop approaches of Stark's group and the motor servo concepts mentioned earlier. All nonlinear constitutive relations were modeled by classic curve fits that are described by a dimensionless shape parameter and a critical point on the relation: the hyperbolic Hill equation (for CE_{fv}), an exponential (for SE and PE) and a Gaussian (for CE_n and SE strain gauge transduction sensitivity). To utilize the dimensionless model, what is needed is l_{m_o}, l_{t_o}, fc_{sl} (fraction slow fibers), and a_{pca} (physiological cross-sectional area), and transmission time delays. Not mentioned was the pennation angle δ, since it is this author's opinion that for δ under 20° (*i.e.*, most muscles), it is not worth splitting up x_{se}; rather, a_{pca} and l_{m_o} can be compensated appropriately, and then during runs, pennation effects can be assumed negligible. If deemed necessary, many geometric mapping variations exist (*e.g.*, Refs. 17, 58, and 68) that yield reasonably similar results, and any can be used to reformulate Eq. 1 terms and remap the output f_m to F_m.

As with all models, many simplifying assumptions were made; some will find the proposed model to be too complex, others overly simple. A model is only as good as its weakest link, given its purpose and scope. One might be inclined to think that the weakest link is related to the rather broad assumptions that were necessary for neurocircuitry-based feedback parameter identification—the classic rationale that modelers have used to justify cutting between muscle mechanics and the MN drive. However, this was not the case, and indeed the process was straightforward once the objective of conservative feedback sculpturing was identified and a decision was made to keep the reference values for the feedback loops very simple. Rather, an intriguing aspect of this study is that there is reasonably high sensitivity to certain *other* strategic modeling assumptions related to mechanics, and especially to IF model properties and to scaling the CE_n and CE_{fv} relations for *submaximal* activation.

The most important decision that was made was to reject the intuitively appealing approach of modeling the IF system as either a position-based spring-like threshold signal or a nonlinear (or linear) unidirectional kinematic transducer. While the former approach is appropriate for postural regulation, and the latter for simulating ramp-and-hold experiments, the fidelity of each for general-purpose voluntary goal-directed movements becomes complex and questionable. Instead, it was assumed that the IF apparatus is composed of muscle tissue that happens to have some embedded strain sensors, and that the concept of α-γ-β linkage is reasonable. This physiologically based, straightforward approach seems to be novel, perhaps because of the unfortunate historical view of spindles as unidirectional kinematic sensors modulated by a γ-drive. IF behavior is fundamentally based on bicausal mechanical interaction between the CE_{IF} and SE_{IF}, with unicausal inputs of γ-drive at one side and the EF length at the other (Fig. 2). This differs from the highly regarded, sophisticated approach of Hasan (16), which clearly captures certain transient behaviors well for the experiments of primary interest. The current IF model is best viewed as a muscle model that is based on a known anatomical infrastructure for the γ_{static} IF system. Under conditions of steady n_{in}, the model predicts spring-like behavior that is similar in magnitude to what is needed for our larger scale shoulder-arm model to replicate the types of postural fields seen experimentally at the hand; and this is without added task-specific feedback. Of note is that the form for choosing the spindle reference signal affects mostly the shifting (or threshold) of the springs, only mildly affecting the quasistatic stiffness despite having a large influence on the transient stiffness. In general, increasing n_r increases cocontraction. This author has shown that while cocontraction increases the transient impedance to external perturbation, it has little effect on a subsequent voluntary movement as long as the antagonist has time to be deac-

tivated appropriately (64,65). Also, as cocontraction levels increase, higher delayed kinematic feedback gains can be tolerated before the system exhibits unstable oscillation. Thus, we see a linkage between general cocontraction and reflex activity, similar to what is commonly seen experimentally (*e.g.*, Ref. 30).

The model also captures basic nonlinear transient ramp-and-hold perturbation effects even when only a simple linear strain transducer is used, because these effects are assumed to be intrinsic to nonlinear bicausal $CE_{IF} - SE_{IF}$ interaction, modulated by γ_{static} drive. It also predicts that during tasks such as isometric contractions, the spindles increase their activity, in line with a wealth of experimental data (*e.g.*, reviews in Refs. 26 and 35).

The present muscle-reflex actuator does not attempt to simulate the subtleties of the nuclear bag_1 fibers. However, given our present emphasis on voluntary movement and posture, the primary (1a) afferent seems less critical. Also, with our posture-based emphasis in developing this IF-chain model, perhaps this approach complements that used for recent IF models (44,48).

Importantly, the decision to treat the IF apparatus as muscle tissue raised some interesting research questions that otherwise would have been missed, and identified a number of areas where further physiological experimental data would be helpful. What is the IF fiber composition? How does the CE_{fl} scale with submaximal activation, and especially the $CE_{fl\text{-}IF}$ during low activations? What is the CE_{fv} relation like in the important low-activation, moderate-to-high lengthening velocity region, especially for the IF muscle? Does IF become slack for the same length as EF? Since muscles with heterogenous sarcomere lengths provide more CE_{fl} excursion (58), might not IF sarcomeres be especially heterogenous? But might this also result in a greater tendency toward yielding, by the "popping" mechanism described by Morgan (41)? Is there a "sticky" (discontinuous) region in the spindle apparatus, as some have proposed (44,48), or is this just a reflection of the $CE_{fv\text{-}IF}$ relation near zero velocity, as suggested here? Is the present type of spindle output, which in a model reference scheme is best compared with a dimensionless measure of efferent neuromotor "state" as opposed to any pure kinematic measure, better or worse for developing higher-level internal model representations?

Ironically, it was not until we were forced to truly address large scale systems that the need for such a synthesized muscle-reflex actuator framework emerged. In addition to simulations for larger scale systems, this new actuator seems especially appropriate for research investigating pathological function from disorders such as Parkinson's disease or cerebral palsy, where changes in tone influence both posture and voluntary movement.

CONCLUSION

The muscle-reflex actuator proposed here offers a reasonable alternative to the approach of using conventional muscle models and then either employing a "final common pathway" input or incorporating sensory feedback in an *ad hoc* manner. It appears to capture the essence of the IF γ_{static}-spindle system, and of the type of conservative autogenic reflex activity that is consistent with "do not intervene" experimental paradigms. Default reflex contributions are reasonably insignificant during voluntary movements, if anything being slightly beneficial due to the parallel EF-IF arrangement. A systematic approach to parameter identification is suggested. Most importantly, for studies of posture in large-scale systems, it provides the type of quasistatic spring-like muscle-reflex behavior that we have found to be necessary. Thus, it is suggested that the key objective has been met: development of a single actuator that can be used for simulations of both movements and posture.

REFERENCES

1. Abbott, B. C., and D. R. Wilkie. The relation between velocity of shortening and the tension-length curve of skeletal muscle. *J. Physiol.* 120:214–223, 1953.
2. Alexander, R. McN., and R. F. Ker. The architecture of leg muscles. In: *Multiple Muscle Systems: Biomechanics and Movement Organization,* edited by J. M. Winters and S. L.-Y. Woo. New York: Springer-Verlag. 1990, pp. 568–577.
3. Bagley, A. M. Analysis of Human Response to Slow Isokinetic Movement. Tempe: Arizona State University, M.S. Thesis, 1987.
4. Bagust, J., S. Knott, D. M. Lewis, J. C. Luck, and R. A. Westerman. Isometric contractions of motor units in a fast twitch muscle of the cat. *J. Physiol.* 231:87–104, 1973.
5. Bahler, A. S. Modeling of mammalian skeletal muscle. *IEEE Trans. Biomed. Eng.* BME-13:248–257, 1968.
6. Daru, K. M. Computer Simulation and Static Analysis of the Human Head, Neck and Torso. Tempe: Arizona State University, M.A. Thesis, 1989.
7. Esbashi, S., and E. Endo. Calcium and muscle contraction. *Progr. Biophys.* 18:123–183, 1968.
8. Ettema, G. J. C., and P. Huijing. Architecture and elastic properties of the series elastic element of muscle-tendon complex. In: *Multiple Muscle Systems: Biomechanics and Movement Organization,* edited by J. M. Winters and S. L.-Y. Woo. New York: Springer-Verlag, 1990, pp. 57–68.
9. Feldman, A. G. Functional tuning of the nervous system during control of movement or maintenance of a steady posture. II. controllable parameters of muscle. *Biophysiology* 11:565–578, 1966.
10. Feldman, A. G., S. V. Adamovich, D. J. Ostry, and J. R. Flanagan. The origin of electromyograms—explanations based on the equilibrium point hypothesis. In: *Multiple Muscle Systems: Biomechanics and Movement Organization,* edited by J. M. Winters and S. L.-Y. Woo. New York: Springer-Verlag, 1990, pp. 195–213.
11. Gielen, C. C. A. M., and J. C. Houk. A model of the mo-

tor servo: incorporating nonlinear spindle receptor and muscle mechanical properties. *Biol. Cybern.* 57:217–231, 1987.
12. Gordon, A. M., A. F. Huxley, and F. J. Julian. The variation in isometric tension with sarcomere length in vertebrate muscles. *J. Physiol.* 184:170–192, 1966.
13. Hannaford, B., and L. Stark. Late agonist burst (PC) required for optimal head movements: a simulation study. *Biol. Cybern.* 57:321–330, 1987.
14. Hannaford, B., and J. M. Winters. Actuator properties and movement control: biological and technological actuators. In: *Multiple Muscle Systems: Biomechanics and Movement Organization,* edited by J. M. Winters and S. L.-Y. Woo. New York: Springer-Verlag, 1990, pp. 69–93.
15. Hannaford, B., J. M. Winters, C.-P. Chou, and P.-H. Marbot. The anthroform biorobotic arm: a system for the study of spinal circuits. *Ann. Biomed. Eng.* 1995, in press.
16. Hasan, Z. A model of spindle afferent response to muscle stretch. *J. Neurophys.* 49:989–1005, 1983.
17. Hatze, H. A general myocybernetic control model of skeletal muscle. *Biol. Cybern.* 28:143–157, 1978.
18. He, J., W. S. Levine and G. E. Loeb. Feedback gains for correcting small perturbations to standing posture. *IEEE Trans. Autom. Control.* 36:322–332, 1991.
19. Hill, A. V. The heat of shortening and the dynamic constants of muscle. *Proc. Roy. Soc.* 126B:136–195, 1938.
20. Hill, A. V. *First and Last Experiments in Muscle Mechanics.* Cambridge, UK: Cambridge University Press, 1970, 140 pp.
21. Hoffer, J. A., and S. Andreasson. Regulation of soleus muscle stiffness in premammilary cats: intrinsic and reflex components. *J. Neurophys.* 45:267–285, 1981.
22. Hogan, N. Adaptive control of mechanical impedance by coactivation of antagonistic muscles. *IEEE Trans. Autom. Control.* AC-29:681–690, 1984.
23. Hogan, N. Principles underlying movement organization: upper limb. In: *Multiple Muscle Systems: Biomechanics and Movement Organization,* edited by J. M. Winters and S. L.-Y. Woo. New York: Springer-Verlag, 1990, pp. 149–164.
24. Hogan, N., and J. M. Winters. Principles underlying movement organization: upper limb and single joint. In: *Multiple Muscle Systems: Biomechanics and Movement Organization,* edited by J. M. Winters and S. L.-Y. Woo. New York: Springer-Verlag, 1990, pp. 182–194.
25. Houk, J. C. Regulation of stiffness by skeletomotor reflexes. *Ann. Rev. Physiol.* 41:99–114, 1979.
26. Houk, J. C., and W. Z. Rymer. Neural control of muscle length and tension. In: *Handbook of Physiology—The Nervous System II,* vol. 8, edited by E.R. Kandel. 1981, pp. 257–323.
27. Joyce, G. C., P. M. H. Rack, and D. R. Westbury. The mechanial properties of cat soleus muscle during controlled lengthening and shortening movements. *J. Physiol.* 204:461–474, 1969.
28. Katz, B. The relation between force and speed in muscular contraction. *J. Physiol.* 96:45–64, 1939.
29. Kleweno, D. G., and J. M. Winters. Effect of initial upper limb alignment on muscle contributions to isometric strength curves. *J. Biomech.* 26:143–153, 1993.
30. Lacquaniti, F., F. Licita and J. F. Soechting. The mechanical behavior of the human forearm in response to transient perturbations. *Biol. Cybern.* 44:35–46, 1982.
31. Lehman, S. L. A detailed biophysical model of human extraocular muscle. Berkeley: University of California, Ph.D. Dissertation, 1982.
32. Lehman, S., and L. Stark. Three algorithms for interpreting models consisting of ordinary differential equations: sensitivity coefficients, sensitivity functions, global optimization. *Math. Biosci.* 62:107–122, 1982.
33. Liddell, E. G. T., and C. S. Sherrington. Reflexes in response to stretch (myotatic reflexes). *Proc. Roy. Soc. Lond.* 96B:212–242, 1924.
34. Lieber, R. L., C. G. Brown, and C. L. Trestik. Model of muscle-tendon interaction during frog semitendinosis fixed-end contractions. *J. Biomech.* 25:421–428, 1992.
35. Loeb, G. E. The control and responses of mammalian muscle spindles during normally executed motor tasks. *Exer. Sport Sci. Rev.* 12:157–204, 1984.
36. Loeb, G. E., and W. Levine. Linking musculoskeletal mechanics to sensorimotor neurophysiology. In: *Multiple Muscle Systems: Biomechanics and Movement Organization,* edited by J. M. Winters and S. L.-Y. Woo. New York: Springer-Verlag, 1990, pp. 165–181.
37. Ma, S., and G. I. Zahalak. Activation dynamics for a distribution-moment model of skeletal muscle. Proc. 6th Conf. Math Modelling, vol. 11. St. Louis, MO, pp. 778–782, 1987.
38. Matthews, P. B. C. Muscle spindles and their motor control. *Physiol. Rev.* 44:219–288, 1964.
39. Matthews, P. B. C. Evidence from the use of vibration that the human long-latency stretch reflex depends upon the spindle secondary afferents. *J. Physiol.* 348:383–415, 1986.
40. Morgan, D. From sarcomeres to whole muscles. *J. Exp. Biol.* 115:69–78, 1985.
41. Morgan, D. Modeling of lengthening muscle: the role of inter-sarcomere dynamics. In: *Multiple Muscle Systems: Biomechanics and Movement Organization,* edited by J. M. Winters and S. L.-Y. Woo. New York: Springer-Verlag, 1990, pp. 46–56.
42. Mussa-Ivaldi, F., N. Hogan and E. Bizzi. Neural, mechanical, and geometric factors subserving arm posture in humans. *J. Neurosci.* 5:2732–2743, 1985.
43. Nashner, L. M., and P. J. Cordo. Relation of automatic postural responses and reaction-time voluntary movements of human leg muscles. *Exp. Brain Res.* 43:395–405, 1981.
44. Otten, E., K. A. Scheepstra, and M. Hulliger. An integrated model of the mammalian muscle spindle. In: *Alpha and Gamma Motor Systems,* edited by A. Taylor and M. Gladden. 1995, in press.
45. Ramos, C. F., and L. W. Stark. Simulation studies of descending and reflex control of fast movements. *J. Motor Behav.* 19:38–61, 1987.
46. Ramos, C. F., and L. Stark. Are detailed models of the muscle spindle appropriate for simulation studies of the stretch reflex? A general method for model comparisons. *Comp. Biomed. Res.* 1995, in press.
47. Rack, P. M., and D. R. Westbury. The short range stiffness of active mammalian muscle and its effect on mechanical properties. *J. Physiol.* 240:331–350, 1974.
48. Schaafsma, A], E. Otten, and J. D. van Willigen. A muscle spindle model for primary afferent firing based on a simulation of intrafusal mechanical events. *J. Neurophys.* 65:1297–1311, 1991.
49. Scott, S. H. Studies of the Morphometry and Mechanical Properties of Mammalian Muscle. Kingston: Queen's University, Ph.D. Dissertation, 1993.
50. Scott, S. H., and G. E. Loeb. The mechanical properties of

the aponeurosis and tendon of the cat soleus muscle during whole-muscle isometric contractions. *J. Morphol.* 1995, in press.
51. Shoemaker, M., and B. Hannaford. A study and model of the role of the Rhenshaw cell in regulating the transient firing of the motoneuron. *Biol. Cybern.* 71:251–262, 1994.
52. Seif-Naraghi, A. H., and J. M. Winters. Effect of task-specific linearization on musculoskeletal system control strategies. 1989 Biomech. Symp. ASME, AMD-98, 1989, pp. 347–350.
53. Stark, L. *Neurological Control Systems*. New York: Plenum Press, 1968, 428 pp.
54. Stein, R. B., and T. Gordon, Nonlinear stiffness-force relationships in whole mammalian skeletal muscles. *Can. J. Physiol. Pharmacol.* 64:1236–1244, 1986.
55. Stein, R. B., and M. N. Oguztoreli. The role of gamma-motoneurons in mammalian reflex systems. *Biol. Cybern.* 39:171–179, 1981.
56. Stephenson, D. G., and D. A. Williams. Effects of sarcomere length of the force-pCa relation in fast- and slow-twitch skinned muscle fibres from the rat. *J. Physiol.* 333:637–653, 1982.
57. Van der Helm, F. C. T. The Shoulder Mechanism: A Dynamic Approach. Delft: Delft University of Technology, Ph.D. Dissertation, 1991.
58. Willems, M. Architectural Heterogeneity and Function of Bi-Articular Muscle. Amsterdam: Free University, Ph.D. Thesis, 1994.
59. Winters, J. M. Generalized Analysis and Design of Antagonistic Muscle Models: Effect of Nonlinear Muscle-Joint Properties on the Control of Fundamental Movements. Berkeley: University of California, Ph.D. Dissertation, 1985.
60. Winters, J. M. Hill-based muscle models: a systems engineering perspective. In: *Multiple Muscle Systems: Biomechanics and Movement Organization,* edited by J. M. Winters and S. L.-Y. Woo. New York: Springer-Verlag, 1990, pp. 69–93.
61. Winters, J. M. Concepts in neuro-muscular modeling. In: *3-D Analysis of Human Movement, Human Kinetics,* edited by P. Allard, I. A. F. Stokes, and J.-P. Blanchi. 1993, pp. 257–292.
62. Winters, J. M., and L. Stark. Analysis of fundamental movement patterns through the use of in-depth antagonistic muscle models. *IEEE Trans. Biomed. Eng.* BME-32:826–839, 1985.
63. Winters, J. M., and L. Stark. Task-specific second-order movement models are encompassed by a global eighth-order nonlinear musculo-skeletal model. Proc. IEEE System, Man and Cybern., Tuscon, AZ, 1985, pp. 1111–1115.
64. Winters, J. M., and L. Stark. Muscle models: what is gained and what is lost by varying model complexity. *Biol. Cybern.* 55:403–420, 1987.
65. Winters, J. M., L. Stark, and A. H. Seif-Naraghi. An analysis of the sources of muscle-joint system impedance. *J. Biomech.* 12:1011–1025, 1988.
66. Winters, J. M., and F. C. T. Van der Helm. A field-based musculoskeletal framework for studying human posture and manipulation in 3D. Proc. of the Symp. on Modeling and Control of Biomed. Sys., Intern. Fed. on Autom. Control., Galveston, TX, 1994, pp. 410–415.
67. Zahalak, G. I. Modeling musclemechanics (and energetics). In: *Multiple Muscle Systems: Biomechanics and Movement Organization,* edited by J. M. Winters, S. L.-Y. Woo. New York: Springer-Verlag, 1990, pp. 1–23.
68. Zajac, F. Muscle and tendon: properties, models, scaling, and application to biomechanics and motor control. *CRC Crit. Review Biomed. Eng.* 17:359–410, 1989.
69. Zajac, F., and J. M. Winters. Modeling musculoskeletal movement systems: joint and body-segment dynamics, musculotendon actuation, and neuromuscular control. In: *Multiple Muscle Systems: Biomechanics and Movement Organizations,* edited by J. M. Winters and S. L.-Y. Woo. New York: Springer-Verlag, 1990, pp. 121–148.